Publications of the Astronomical Society of the Pacific, 138:034102 (10pp), 2026 March https://doi.org/10.1088/1538-3873/ae4a4c
© 2026. The Author(s). Published by IOP Publishing Ltd on behalf of the Astronomical Society of the Pacific (ASP).

OPEN ACCESS

Effects of Varied Cosmic Ray Feedback from AGN on Massive Galaxy Properties

Charvi Goyal[1], Sam B. Ponnada[1,2], Philip F. Hopkins[1], Sarah Wellons[3], Jose A. Benavides[4], and Kung-Yi Su[5]
[1] TAPIR, California Institute of Technology, Mailcode 350-17, Pasadena, CA 91125, USA
[2] Department of Space, Earth and Environment, Chalmers University of Technology, Gothenburg, Sweden
[3] Department of Astronomy, Van Vleck Observatory, Wesleyan University, 96 Foss Hill Drive, Middletown, CT 06459, USA
[4] Department of Physics and Astronomy, University of California, Riverside, 900 University Avenue, Riverside, CA 92521, USA
[5] Department of Physics & Astronomy and Center for Interdisciplinary Exploration and Research in Astrophysics (CIERA), Northwestern University, 1800 Sherman Ave, Evanston, IL 60201, USA
Received 2025 December 11; revised 2026 February 7; accepted 2026 February 25; published 2026 March 25

Abstract

Active galactic nuclei (AGN) provide energetic feedback necessary to "turn off" star formation in high-mass galaxies ($M_{\rm halo} \geqslant 10^{12.5}\ M_\odot$, $10.4 \leqslant \log(\frac{M_*}{M_\odot}) \leqslant 11$) as observed. Cosmic rays (CRs) have been proposed as a promising channel of AGN feedback, but the nature of CR feedback from AGN remains uncertain. We analyze a set of high-resolution simulations of massive galaxies from the Feedback in Realistic Environments (FIRE-3) project including multi-channel AGN feedback, explicitly evolving kinetic/mechanical, radiative, and spectrally-resolved CRs from the central black hole. Specifically, we explore different CR feedback and transport assumptions, calibrated to Milky Way local ISM constraints, and compare them to observed galaxy scaling relations. We find that all parameterizations explored self-regulate within agreement with observed galaxy scaling relations, demonstrating that CR injection efficiencies varied by $\sim$1.5 dex and locally-variable transport produce quenched galaxies with reasonable bulk properties; however, they feature orders-of-magnitude variant circumgalactic medium gas properties. Our results indicate that multi-wavelength synthetic observations probing these varied halo properties from larger simulated samples in conjunction with observational comparisons may place novel constraints on how AGN physically quench star formation in massive galaxies.

Unified Astronomy Thesaurus concepts: Active galactic nuclei (16); Cosmic rays (329); Magnetohydrodynamical simulations (1966); Supermassive black holes (1663); Galaxy evolution (594); Galaxy quenching (2040); AGN host galaxies (2017); Circumgalactic medium (1879)

1. Introduction

The "quenching problem" of massive galaxies has been a longstanding discrepancy in galaxy formation between observed star formation rates and those predicted by simulations in massive galaxies (Cole et al. 2002; Springel & Hernquist 2003; Longair 2008; Kereš et al. 2009; Benson 2010; Hopkins et al. 2023). Galaxies with high dark matter halo masses ($M_{\rm halo} \gtrsim 10^{12.5}\ M_\odot$) appear "red and dead" and are observed to have less gas cooling than predicted (Benson 2010). It is well-established that feedback processes play a vital role in preventing gas from cooling down and collapsing into stars (Silk & Rees 1998; Hopkins et al. 2004; Croton et al. 2006; Croton & Farrar 2008; Longair 2008; Benson 2010; Hopkins et al. 2018), rectifying this 'overcooling problem; however, the specific mechanisms by which quenching occurs remain unclear.

Due to their immense mass and energy output, Active Galactic Nuclei (AGN) are thought to be critical suppressors of gas cooling in the interstellar medium (ISM), circumgalactic medium (CGM) and intracluster medium (Silk & Rees 1998; Croton et al. 2006; Longair 2008; Somerville & Davé 2015; Su et al. 2021). Several studies have found that models with AGN feedback channels are necessary to explain massive galaxy properties when compared to non-AGN counterparts (Harrison et al. 2018; Su et al. 2019, 2021; Hopkins et al. 2023; Wellons et al. 2023), which is why most modern simulations which aim to reproduce the observed bulk properties of galaxies in a statistical manner include AGN feedback (Schaye et al. 2014; Sijacki et al. 2015; Somerville & Davé 2015; Davé et al. 2019; Su et al. 2019).

How energy from AGN is transferred and coupled to the gas of the host galaxy is now the major open question. Motivated by observations, most of the theoretical literature has focused on the radiative and mechanical feedback modes

Original content from this work may be used under the terms of the Creative Commons Attribution 4.0 licence. Any further distribution of this work must maintain attribution to the author(s) and the title of the work, journal citation and DOI.

of AGN (see Harrison & Almeida 2024, for a recent review). Observed UV and X-ray emission from AGN suggest that AGN generate strong radiation fields due to accretion, which can Compton-heat, photo-ionize, and drive winds via radiation pressure. AGN also drive mechanical outflows and jets (for reviews, see Fabian 2012; Heckman & Best 2014), which can evacuate large cavities and thermalize energy via shocks and turbulent mixing.

AGN are also prodigious sources of cosmic rays (CRs), seen in synchrotron, γ-ray, and inverse Compton emission, which could affect surrounding gas via ionization, heating, or large-scale non-thermal pressure gradients in galactic halos (Butsky & Quinn 2018; Su et al. 2020; Hopkins et al. 2020b; Bustard & Zweibel 2021). How these different channels influence quenching is a topic of ongoing study in galaxy formation (Benson 2010; Somerville & Davé 2015; Su et al. 2020, 2021, 2024; Wellons et al. 2023; Byrne et al. 2024).

Recent progress in galaxy evolution simulations has allowed for higher hydrodynamic resolution and explicit modeling of different AGN feedback modes, most recently including CRs, along with their dynamical, thermo-chemical, and radiative couplings to gas (Hopkins et al. 2023). While some studies have found CRs to be a promising AGN feedback mechanism (Ruszkowski et al. 2017; Su et al. 2020; Wellons et al. 2023), the details of CR production by AGN and how CRs feedback couples to the host galaxy and surroundings are largely unknown theoretically, and the plausible parameter space remains vast, largely owing to the order-of-magnitude uncertanties in the CR scattering rate (related to sub-AU structure of magnetic fields in halos), which manifests in the CR diffusion/streaming parameters (Ruszkowski & Pfrommer 2023; Byrne et al. 2024; Ponnada et al. 2025; Hopkins 2025).

In this study, we explore the orders-of-magnitude variable parameter space of CR feedback from AGN and show that these models reasonably reproduce observed properties of high-mass galaxies ($M_{\rm halo} \approx 10^{13}\,M_{\odot}$), but crucially differ in their CGM properties, potentially allowing for constraints on these "micro-physical" parameters via emergent observables. We use cosmological zoom-in, cosmic-ray-magneto-hydrodynamic (CR-MHD) galaxy formation simulations from the Feedback In Realistic Environments project (FIRE-3)[6] (Hopkins et al. 2023), which allows for a more advanced treatment of CR and black hole physics. The relevant physical parameters we vary reflect the uncertainties in CR physics on small, unresolved scales on the scales of CR gyro-radii in terms of their transport (parameterized by prescriptions for the effective macroscopic scattering rate, which gives rise to diffusion- and streaming-like behaviors) and how efficiently CRs are produced by AGN, i.e., the percentage of AGN accretion energy that is output in the form of CRs. In Section 2, we describe our suite of simulations and analysis methodology before presenting our analysis of the simulations and their properties in Section 3. Finally, in Section 4, we discuss and conclude our findings.

[6] https://fire.northwestern.edu/

2. Methods

2.1. Simulations

We analyze a set of FIRE-3 cosmic-ray-magnetohydrodynamic (CR-MHD), cosmological zoom-in simulations, evolved with the `GIZMO` hydrodynamics solver in meshless-finite-mass mode (Hopkins 2015). All simulations include standard FIRE-3 physics and methods as detailed in Hopkins et al. (2023). We model star formation in self-gravitating, Jeans-unstable gas. Explicit stellar evolution follows feedback arising from radiation pressure, Type I and II supernovae, stellar winds from OB and AGB stars, photoionization, and photo-electric heating. Stellar feedback is coupled to multi-band (extreme UV to far-infrared) radiation and gas cooling from 1 to 10^{10} K. This, in conjunction with numerical resolution ($M_{\rm gas} \sim 3 \times 10^5\,M_{\odot}$) naturally gives rise to a multi-phase interstellar and circumgalactic medium.

All simulations include magnetic fields and anisotropic transport and viscosity, using MHD methods described in Hopkins & Raives (2015) and Hopkins et al. (2016). The cosmic ray physics is coupled directly to the magnetohydrodynamics, with the full CR spectrum of MeV–TeV protons and electrons propagated along magnetic field lines according to the fully general CR transport equations, and interacting with the gas via scattering, Lorentz forces, and all relevant loss terms (e.g., radiative, catastrophic, adiabatic, streaming, re-accleration), as described in Hopkins et al. (2022a). CRs from SNe and fast stellar winds are injected with 10% of the initial SNe/wind kinetic energy and a power-law injection spectrum motivated by diffusive shock acceleration.

Our simulation suite consists of 4 sets of m13 (in reference to their dark matter halo mass $M_{\rm halo} \sim 10^{13}\,M_{\odot}$) FIRE galaxies. The four m13 halos are `h206` (some variations of which were explored in Byrne et al. 2024; Ponnada et al. 2025), `h113`, `h029`, and `h236`. These simulations all include black holes (BHs) and their explicit associated radiative, mechanical, and cosmic ray feedback modes following Hopkins et al. (2023); we refer the reader to details therein regarding those feedback channels.

In brief, BH mechanical feedback utilizes a hyper-refined particle spawning method, with particles of $\sim$1000 times higher resolution (lower particle mass) initiated preferentially along the angular momentum axis of the BHs (as perfectly collimated jets) before de-refinement upon mixing into the surrounding gas cells via reaching the local sound speed. All simulations explored in this study utilize initial mechanical wind velocities of 3000 km s^{-1} and a total coupled photon momentum flux (L/c) of 1.

Table 1
Properties of the FIRE-3 Simulation Suite Analyzed in This Work

Halo	Model	$\epsilon_{\rm cr}^{\rm BH}$ (10^{-4})	$\log_{10}(M_{\rm halo})$ ($M_\odot$)	$\log_{10}(M_*)$ ($M_\odot$)	$E_{\rm cr}^*$ (10^{58} erg)	$E_{\rm cr}^{\rm BH}$ (10^{58} erg)
h206	CD	3	12.7	10.9	10.74	33.22
h206	VDLoCR	1	12.7	10.9	8.78	4.94
h206	VDMidCR	10	12.7	10.8	7.03	7.12
h206	VDHiCR	30	12.7	10.4	3.21	5.15
h113	CD	3	12.8	11.2	19.03	63.28
h113	VDMidCR	10	12.8	11.0	12.48	9.99
h029	CD	3	13.0	11.4	29.5	27.95
h029	VDMidCR	10	13.0	11.1	15.9	16.28
h236	CD	3	13.1	11.0	11.42	38.2
h236	VDMidCR	10	13.1	10.9	8.76	13.31

Note. The columns, from left to right, are: name of the halo evolved in FIRE-3, the CR model used to evolve it, energy efficiency of CR injection by the AGN, halo mass, stellar mass, and the total CR energy produced by stars by $z = 0$, and the total CR energy produced by the AGN by $z = 0$. "VD" models have a variable diffusion coefficient derived from ISM properties whereas "CD" models have a constant power-law diffusion coefficient. The prescription with which stellar and halo mass are defined is described in more detail in Section 2.2. The specific prescription used to calculate total CR energy by source is described in detail in Section 2.3. VD runs have less CR production than their CD counterparts, and less AGN feedback relative to the amount of stellar feedback.

Each of the four halos was evolved with different CR physics models, varying the energy fraction of AGN accretion that is injected as CRs and the CR transport model. The energy fraction determines the rate of energy injected from the AGN into surrounding gas cells as CRs (with the same injection spectrum as from SNe) whenever mechanical energy is deposited as follows:

$$\dot{E}_{\rm cr}^{\rm BH} \equiv \epsilon_{\rm cr}^{\rm BH} \dot{M}_{\rm BH} c^2$$

where $\dot{E}_{\rm cr}^{\rm BH}$ is the CR injection energy rate, $\epsilon_{\rm cr}^{\rm BH}$ is the energy fraction, and $\dot{M}_{\rm BH}$ is the black hole accretion rate (Hopkins et al. 2023).

The two CR transport models we explore are: (1) a temporally and spatially constant power-law scattering rate, which gives rise to an effective diffusion coefficient as a function of CR rigidity (R) of $\kappa_{\rm eff} \sim R^{0.6}$, hereafter referred to as "CD," and (2) a variable diffusion coefficient dependent on the ISM properties, motivated by the "external driving" model as described in Hopkins et al. (2022b) to calibrate scattering rates to reproduce Voyager and AMS-02 observations in Milky Way-mass FIRE-3 simulations, hereafter referred to as "VD." The VD model is similar in principle to scattering models predicted by "extrinsic turbulence" models (Jokipii 1966), however, with the empirically-motivated addition of a turbulent driving term at gyro-resonant wave-numbers to reproduce the correct spectral shapes in Milky Way Solar Circle-like conditions. This model in principle can produce different scattering and thus CR transport properties from the Milky Way local ISM in different plasma conditions characteristic of the ISM/CGM of massive galaxies explored here.

We pair the VD model with three CR injection efficiencies: 1×10^{-4} (low), 1×10^{-3} (medium), and 3×10^{-3} (high), hereafter referred to as "VDLoCR," "VDMidCR," and "VDHiCR," respectively. We summarize the simulations analyzed in Table 1.

2.2. Derived Quantities

We calculate several bulk galaxy properties for each simulation, by the same prescriptions as Wellons et al. (2023) and Byrne et al. (2024). Halo mass is defined as the total mass inside the virial radius. Virial radius (R_{200}) is determined by the radius where the average density equals 200 times the critical density of the Universe ($\rho_{\rm c} = 3{\rm H}^2/8\pi{\rm G}$). The stellar mass is computed as the total mass of stars within 50 kpc of the galaxy's center, where the galaxy center is defined by the location of the central supermassive black hole (SMBH). For all snapshots, we orient the galaxies face-on using the angular momentum vector of the star particles to define the rotation axis, and transform all cell vector fields accordingly.

We then measure the 300 Myr averaged star formation rate (SFR) at $z = 0$ as the total mass of stars formed in the last 300 Myr within 50 kpc, averaged over that timescale. The effective radius, defined as the two-dimensional radius enclosing half of the stellar mass when the galaxy is viewed

face-on, is used to calculate the velocity dispersion of stars, σ, which is defined as the standard deviation of the z-velocity of stars within the effective radius.

2.3. Cosmic Ray Injection Histories

In addition to bulk properties, we calculate the CR injection rates from stellar sources and AGN for each run until $z = 0$. We first calculate the time-series SFR as the total mass of star particles formed within 50 kpc of the galactic center, corrected for mean mass loss rates to obtain the at-formation stellar mass (Hopkins et al. 2023). From there, we approximate the stellar CR injection rate as $\dot{E}_{\rm cr}^{*} \approx 0.1 \times 10^{51}\,{\rm erg}\,(\dot{M}_{*}/100 M_{\odot})$, where 0.1×10^{51} erg is the amount of CR energy released from a single supernova event, which occurs approximately once per $100\,M_{\odot}$ of the stars formed. To obtain the cumulative CR energy injected into the galaxy by stellar feedback, we integrate the injection rate over time. We use the AGN accretion rate to calculate the CR injection rate from the AGN, where $\dot{E}_{\rm cr}^{\rm BH} \equiv \epsilon_{\rm cr}^{\rm BH} \dot{M}_{\rm BH} c^2 \approx 1.8 \times 10^{59}\,{\rm erg}\,(\dot{M}_{\rm BH}/10^{8} M_{\odot})(\epsilon_{\rm cr}^{\rm BH}/10^{-3})$. We cumulatively integrate the time-series injection rates over time for each source to find the cumulative CR energy injected into the galaxy by each source.

2.4. Radial Profiles

Finally, we analyze various radial profiles for each simulation snapshot. The CR energy density profiles at different redshifts are computed as the total CR energy contained in shells of $\sim$1.7 kpc thickness at a given radius away from the galaxy's center, divided by the volume of each shell. Following a similar procedure, we also generate gas number density and effective CR diffusion coefficient ($\kappa_{\rm eff}$) profiles for different redshifts. To calculate $\kappa_{\rm eff}$, we first average the diffusivity of the $\sim$0.1–100 GeV proton spectrum by taking the energy-weighted mean of the diffusivities of the spectral bins for each given cell. Then, we use the aforementioned volume-weighting to obtain a radial profile of $\kappa_{\rm eff}$.

3. Results

3.1. Bulk Properties

The bulk properties of the galaxies are plotted in Figure 1, and show that the models produce galaxies that are in agreement with known empirical scaling relations.

The top panel shows the stellar mass–halo mass (SMHM) relation, tracking the amount of star formation regulation. The galaxies are compared to the median observational SMHM found by Behroozi et al. (2019) of central galaxies (both star-forming and quenched), following Wellons et al. (2023), with galaxies within 0.5 dex of the line being considered as properly regulated. All models explored here produce galaxies that

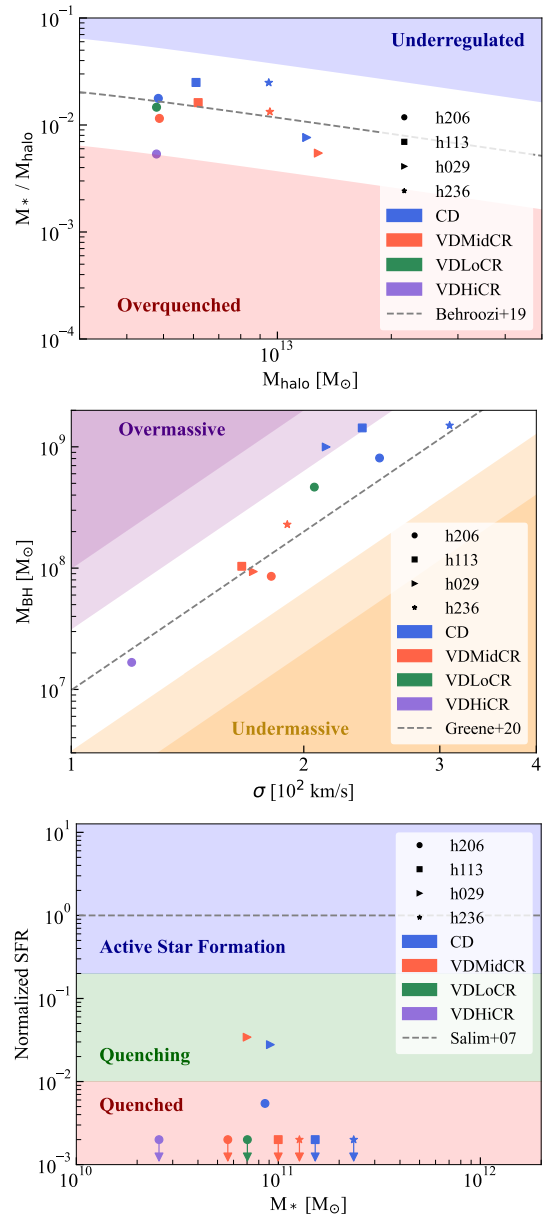

Figure 1. Scaling relations for all `h206`, `h113`, `h029`, and `h236` runs at $z = 0$, indicated by squares, circles, triangles, and stars, respectively. Blue, green, red, and purple markers indicate runs with the CD, VDLoCR, VDMidCR, and VDHiCR model, respectively. Irrespective of the details of CR physics, all models produce well-regulated, quenched galaxies with reasonable SMBH masses, in agreement with the scaling relations. Top: The stellar mass–halo mass relation from Behroozi et al. (2019) (dashed line). The blue and red regions describes galaxies with under-regulated and over-quenched stellar populations respectively. Center: The $M_{\rm BH}$-σ relation from Greene et al. (2020) (dashed line). The purple and orange regions describes galaxies with overly-massive and undermassive AGN respectively, with ± 0.5 to $\pm$ 1 dex region filled with light purple and orange and the regions more than a dex away filled with dark purple and orange. Bottom: The 300 Myr averaged star formation rate, normalized to the median value of star formation observed in star-forming galaxies at $z = 0$ from Salim et al. (2007). The blue, green, and red regions describe actively star-forming, quenching, and quenched galaxies.

fall within the range of being well-regulated. As might be expected, higher cosmic-ray injection efficiency (stronger feedback) leads to stronger suppression of star formation. VD models produce galaxies with stronger suppression than the CD model, including the VDLoCR run of h206, despite it having a lower CR injection efficiency than the CD model. We also note that $M_{\rm halo}$ has little variation across models for each halo, producing a qualitatively distinct vertical band for each halo in the panel.

In the middle panel of Figure 1, we show the $M_{\rm BH}$–σ relation at $z = 0$, where σ refers to the velocity dispersion of stars, as described in Section 2.2. The models are compared with the observational relation of Greene et al. (2020), with the model SMBH considered to be properly massive if the mass is within the 0.5 dex intrinsic scatter of the observational constraint and reasonable if within 1 dex. All models we explore follow this relation, with two CD runs, h113 and h029, sitting right outside of the intrinsic scatter of the constraint. Models with higher cosmic-ray injection efficiencies are seen producing galaxies with lower AGN mass and velocity dispersion, suggesting that the stronger the CR feedback, the more AGN growth is suppressed, corresponding with the same trend as seen in the SMHM relation. However, the CD model produces galaxies with the highest black hole mass despite having higher CR efficiency than VDLoCR, suggesting that variable CR transport is more efficient at suppressing BH growth for a given energy injection, potentially via stronger confinement of the CRs in the inner CGM. The $M_{\rm BH}$-σ relation also appears to be less sensitive to variations in initial halo conditions, producing a cluster for each specific model across different halos.

The bottom panel shows the 300 Myr averaged SFR of each model variation and halo at $z = 0$, normalized to the median star formation expected from a star-forming main sequence galaxy (including AGN/SF composite galaxies) at $z = 0$ as found by Salim et al. (2007), against the stellar mass to measure star formation suppression. All runs are at least 1 dex below the expected SFR for actively star-forming galaxies, and most are at least 2 dex below, indicating that the galaxies are quenched. VD models appear to have marginally higher $z = 0$ SFRs but lower stellar masses than their CD counterparts for the same halo. Thus, we find that all CR parameterizations explored yield reasonably quenched galaxies with appropriate stellar and black hole masses at this halo mass scale.

3.2. Cosmic Ray Injection Histories and Implications for Quenching

Similarly to Byrne et al. (2024), we approximate the total energy of CRs produced from stars over the age of the universe as $E_{\rm cr}^{*} \approx 0.1 \times 10^{51}{\rm erg}\,(M_{\rm sf}/100 M_{\odot})$, where 0.1×10^{51} erg is the amount of CR energy released from a single supernova event, which occurs approximately once per 100 $M_{\odot}$ of the stars formed, and $M_{\rm sf}$ is the cumulative at-formation stellar mass (see Section 2.4 for more detailed methodology). Similarly, we approximate the total CR energy produced by the AGN as $E_{\rm cr}^{\rm BH} = \epsilon_{\rm cr}^{\rm BH} M_{\rm BH,acc} c^2 \approx 1.8 \times 10^{59}{\rm erg}\,(M_{\rm BH,acc}/10^{8} M_{\odot})(\epsilon_{\rm cr}^{\rm BH}/10^{-3})$ where $M_{\rm BH,acc}$ is the cumulative mass accreted onto the AGN. Table 1 summarizes the cumulative CR energy deposited from each source by $z = 0$ for all runs in our simulation suite.

We find that while VD runs have at most ~1.6 times more CR energy from AGN feedback compared to stellar feedback, the CD runs have up to ~3.3 times the CR energy from AGN versus stellar sources. The CD runs produce more CR energy from both stars and the AGN compared to VDMidCR across all halos, despite having a lower injection efficiency.

This is because the VD transport models control BH growth more effectively than CD. Moreover, this indicates that the primary way in which the increased CR feedback efficiency regulates galaxy growth is not via aggregate injection of CRs, but rather due to the *timing* of injection, which is inherently chaotic and sensitive to the "responsiveness" of the BH feedback model, as described in Wellons et al. (2023).

Interestingly, we also find that while $E_{\rm cr}^{*}$ decreases linearly with CR injection efficiency in h206's VD runs, $E_{\rm cr}^{\rm BH}$ peaks with VDMidCR, highlighting the same non-linear behavior of increasing CR feedback efficiency as seen in the CR energy density profiles in the CGM at $z = 0$ (Figure3). This potentially indicates a threshold-like behavior from a largely feedback-regulated to a mostly fueling-regulated regime.

We calculate the CR injection rates from stellar and AGN feedback for the h206 runs and present them in Figure 2. We find increasing variability in AGN injection rates for VD models with increasing injection efficiency, indicating higher responsiveness of the feedback model. The CD model produces AGN injection rates systematically higher than those of VDLoCR after ~5 Gyr despite having similar profiles before then. Note again, the CD model has a factor of 3 higher CR injection efficiency than that of VDLoCR and a factor of ~6.7 larger total $E_{\rm cr}^{\rm BH}$ and despite this, the VDLoCR model exhibits stronger regulation on the scaling relations (Figure 1). This indicates that the CR transport variation alone can play a significant role in the responsiveness of a given AGN feedback model.

The VDMidCR and VDHiCR runs have slightly earlier initial AGN injection times and exhibit higher variation in AGN injection rates at late times, but still on average lower than that of the CD model. As expected, stellar CR injection rates are relatively low compared to star-forming galaxies after quenching past ~6 Gyr, with brief bursts typically subdominant to the BH contribution. This indicates all models primarily regulate via AGN feedback, and more so that they are regulated via its responsiveness, here particularly that of the CR feedback model (Wellons et al. 2023).

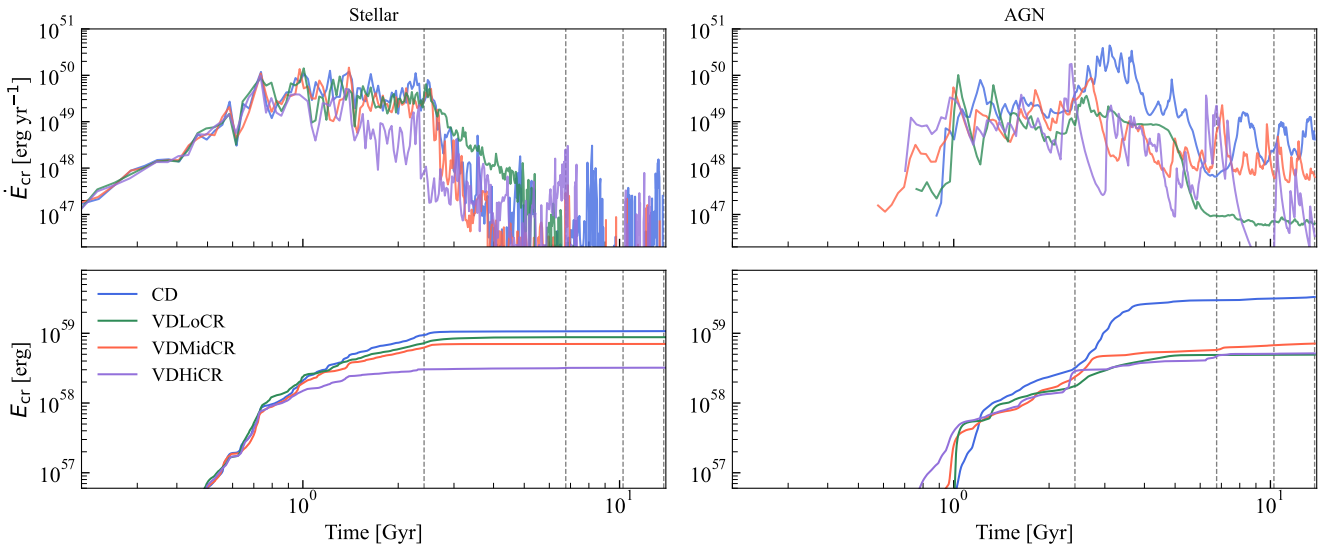

Figure 2. Cosmic ray injection rate (top) and cumulative injected energy (bottom) by source of the `h206` runs, from 0 to 13.8 Gyr. Stellar feedback is plotted on the left; AGN feedback is plotted on the right. Vertical dashed lines correspond to snapshots showcased below in Figures 3–5. The injection rate is binned at ∼30 Myr intervals for both stellar and AGN injection. The stellar injection rate is obtained by rescaling the star formation history, $\dot{E}^{*}_{\rm cr} \approx 0.1 \times 10^{51}{\rm erg}(\dot{M}_{\rm sf}/100 M_{\odot})$. The AGN injection rate is obtained by rescaling the AGN accretion history by the injection efficiency specific to the model used, $\dot{E}^{\rm BH}_{\rm cr} \approx 1.8 \times 10^{59}{\rm erg}(\epsilon^{\rm BH}_{\rm cr}/10^{-3})(\dot{M}_{\rm BH,acc}/10^{8} M_{\odot})$. Stellar injection rate is relatively steady-state after ∼6 Gyr with respect to star-forming galaxies. All runs exhibit a moving average in AGN injection rate. VDMidCR has the earliest AGN-projected CR injection and has both the highest injection rate and cumulative injection at 13.8 Gyr compared to the other VD runs. Unlike other runs, VDLoCR's AGN injection rate stabilizes beyond ∼6 Gyr.

We note here also that the self-regulation our simulated galaxies exhibit is non-trivial. In Figure 1, we showed that for increasing CR feedback efficiency, `h206` runs *moved down* the $z = 0$ SMHM relation while moving *along* the $M_{\rm BH}$–σ relation. In the feedback-regulated BH growth picture (Di Matteo et al. 2005; Sijacki et al. 2007, 2009), accretion onto the BH gets shut down due to "quasar-mode" feedback, which is more ejective & explosive in nature. This is evinced by the similar $E^{\rm BH}_{\rm cr}$ injected by each VD model, and their subsequent $M_{\rm BH}$ which corresponds inversely to $\epsilon^{\rm BH}_{\rm cr}$.

Subsequently, evolution enters a "fueling-regulated" mode (commonly referred to or implemented as "radio-mode" feedback; Weinberger et al. 2018) where $M_{\rm BH}$ changes slowly and star formation is modulated by prevention of gas accretion. This "maintenance-mode" allows for M_{*} to further change, modifying the central potential and thus σ, moving points down the SMHM relation and along the $M_{\rm BH}$–σ relation. We have verified this qualitative behavior by examining the $M_{\rm BH}$–σ relation for each individual snapshot (see Figure A1 in the Appendix).

Importantly, in our simulations here, we have not inserted "by hand" any qualitative change in the feedback prescription for varied Eddington ratios as in large-volume cosmological simulations—the halos' collective response to feedback naturally arises from the coupling of feedback to gas, which varies in its responsiveness, and the cosmological assembly of the galaxies. This highlights how multi-channel AGN feedback, varied solely in CR efficiency, can naturally produce *both* qualitative feedback behaviors necessary to reproduce bulk massive galaxy observables.

3.3. CGM Properties

In this subsection, we present radial profiles of various physical quantities in the CGM from our simulations. We find that all halos produce similar qualitative profile trends for a given physics variation, so we focus on `h206` hereafter. The radial profiles of CR energy density are shown in Figure 3. Different models exhibit different radial profiles of CR energy density $e_{\rm cr}$, or equivalently the CR pressure since $P_{\rm cr} \approx \frac{1}{3} e_{\rm cr}$ for $\gamma_{\rm cr} = 4/3$. In particular, CD and VD models evolve differently with time, with the CD model presenting a power-law-like profile at late times and VD models exhibiting qualitatively flatter radial profiles, particularly at late times. For the VD models of varied injection efficiency, we find that the CR energy density profiles in the CGM at $z = 0$ exhibit a nonlinear ordering, where the VDMidCR model has the highest $e_{\rm cr}$ among all VD models at radii $\gtrsim$15 kpc. The VDHiCR model produces the largest variation in its $e_{\rm cr}$ profile over time, having the lowest $e_{\rm cr}$ in the inner halo at the earliest time ($\tau = 2.4$ Gyr) followed by the highest inner halo $e_{\rm cr}$ at $\tau = 6.8$ Gyr among the VD models and then decreasing to the lowest energy density at $z = 0$, with its CGM $e_{\rm cr}$ nearly an order of magnitude lower at a given radius than that of VDMidCR and VDLoCR models at $z = 0$.

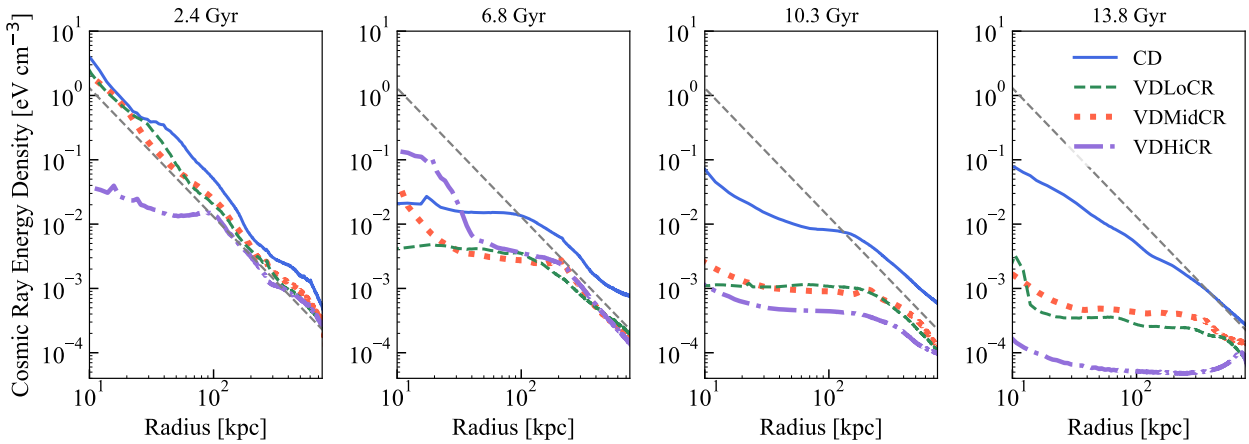

Figure 3. Radial profiles of the volume-weighted mean e_{cr} in the halos of the `h206` runs, binned in ∼1.7 kpc spherical annuli. Snapshots at $\tau = 2.4$, 6.8, 10.3, 13.8 Gyr are shown in the left to right panels respectively. The gray dashed line is the $1/r^2$ profile expected from steady state CR injection and $\kappa_{\rm eff} \propto r$ (Butsky et al. 2023). VD models have increasingly flatter profiles over time, with a nonlinear relationship between the normalization of the e_{cr} profiles and CR injection efficiencies ($\epsilon_{\rm cr}^{\rm BH}$).

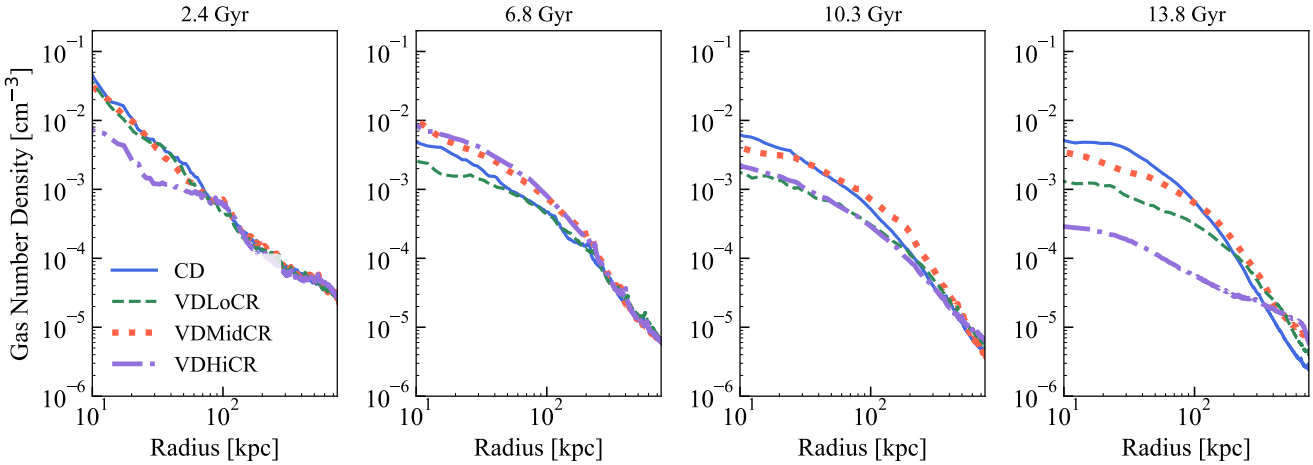

Figure 4. Radial profiles of the volume-weighted mean $n_{\rm gas}$ for the `h206` runs, from 10 to 750 kpc binned in ∼1.7 kpc spherical annuli. Snapshots at $\tau = 2.4$, 6.8, 10.3, 13.8 Gyr are shown in the left to right panels respectively. Similar trends as the CR density profile suggest dynamical coupling of CRs to gas.

The VDHiCR model exhibits a similar trend over time in its radial profile of gas number density (Figure 4). At $z = 0$, the gas density radial profiles share the same ordering with CR injection efficiency as CR energy density does; in general, CGM gas density profiles appear to flatten over time irrespective of the model variation, particularly within $r \lesssim 300$ kpc (out to the approximate virial radii of these halos). The similarities between the CGM gas density and CR energy density owe to the dynamical coupling of CRs to the gas, as steep gradients in e_{cr} at the edge of flattened "shelves" in the profiles aid in outflows.

Since the CRs can diffuse, and the CR pressure is time-dependent, the shelves in e_{cr} can move ahead of the gas (Hopkins et al. 2021; Ponnada 2025), and so e_{cr} as a function of radius (or gas density) does not appear to trace this exact, tightly-coupled adiabat (Hopkins et al. 2022a). Despite this, and even though these halos are not CR pressure dominated overall, there appears to be some degree of spatial correspondence between the gradual flattening of e_{cr} with time shown in Figure 3 and the qualitative dilution and flattening of the gas density profiles with time in Figure 4, particularly in the VDHiCR case which has the largest modulation in AGN-injected e_{cr} over time.

In Figure 5, we show the radial profiles of the volume-weighted mean CR *effective* diffusion coefficient (which is itself energy-averaged over all CR energy bins for each gas cell; see Section 2), $\kappa_{\rm eff}$, at different redshifts. Here, $\kappa_{\rm eff}$ contains both "diffusion-like" and "streaming-like" terms which emerge from the evolved scattering rate as a function of rigidity, $\nu_{\rm cr}(R)$, but *not* the advective transport of CRs. The CD model, as expected, has a largely constant effective diffusivity, with slight changes representing small shifts in the

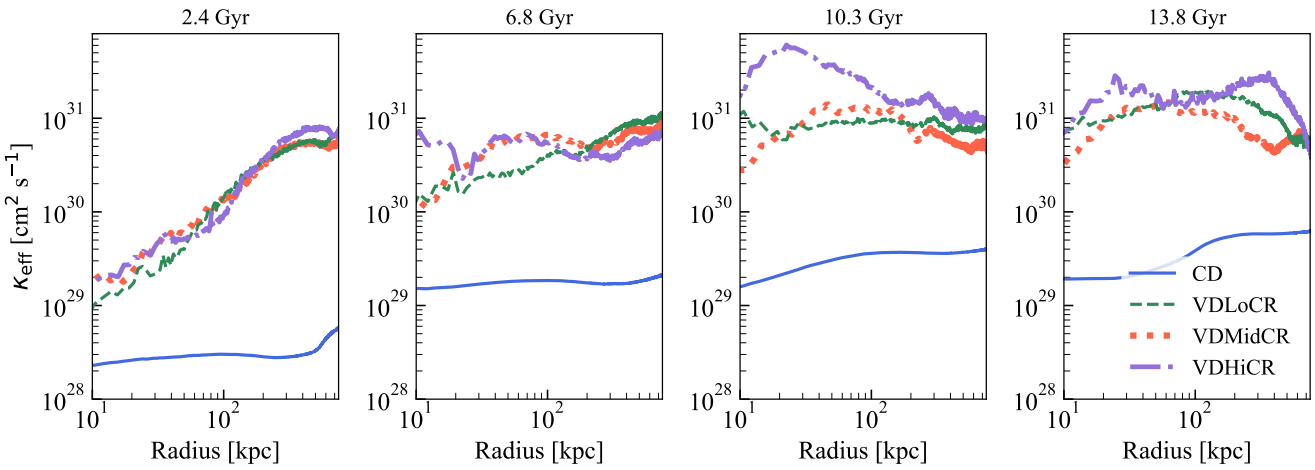

Figure 5. Radial profiles of the volume-weighted mean cosmic ray diffusivity $\kappa_{\rm eff}$ in the halos of the `h206` runs, from 10 kpc to 750 kpc binned in ∼1.7 kpc annuli. Snapshots at $\tau = 2.4$, 6.8, 10.3, 13.8 Gyr are shown in the left to right panels respectively. The presences of troughs suggests the possibility of CR winds.

CR energy spectrum from the canonical ∼GeV peak at a given radius. Moreover, the "troughs" present in the VD profiles correspond to areas of lower diffusivity surrounded by high diffusivity that could trap CRs, thus creating local $e_{\rm cr}$ over-densities. Indeed, we see such troughs in $\kappa_{\rm eff}$ correspond to local over-densities in $e_{\rm cr}$ in Figures 3 and 5 e.g., in VDHiCR at ∼15 kpc and ∼200 kpc at $\tau = 6.8$ Gyr; in VDMidCR at ∼200 kpc at $\tau = 10.3$ Gyr and ∼400 kpc at $\tau = 13.8$ Gyr; and in VDLoCR at ∼15 kpc at $\tau = 10.3$ Gyr. Sharper troughs correspond to stronger local CR pressure gradients and over-densities.

We note here that at the earliest times just after the period of the most rapid BH growth (for instance at $\tau = 2.4$ Gyr), all of the models' CGM properties in Figures 3–5 are more similar than they are different, which is particularly true of the VD runs, though with some differences in the inner $e_{\rm CR}$ profiles set by the earliest "feedback-regulated" phase. Much of the differences in the CGM properties at $z \sim 0$ are instead set by the behavior of the models at later times during the "maintenance-mode" phase of growth.

4. Discussion and Conclusions

In this work, we have explored plausible models for AGN feedback with varied CR injection efficiencies from the black hole, and two different CR transport models. All parameterizations of CR physics explored here produce reasonable galaxies with suppressed star formation rates, suggesting that bulk properties of the galaxies are relatively insensitive to CR parameterizations. However, the radial profiles of CR energy density and gas properties reveal differences in model predictions, which may reveal an avenue to constrain how AGN feedback regulates galaxies, and particularly, the role of CRs in quenching.

The CR energy density profiles are flatter than expected from a constant injection of CRs and steady-state halo CR pressure (Butsky et al. 2023), which owes to the time-dependent nature of the injection. Ponnada (2025) show that time-dependent injection of CRs (decreasing $\dot{E}_{\rm cr}$ with time) undergoing a mix of diffusive- and streaming/advection-like transport leads to flattening of $P_{\rm cr}(r)$ relative to time-steady expectations.

Indeed, this behavior is shown in Ponnada (2025) for the same CD run of `m13h206` we analyze here and agrees well with time-dependent analytic expectations. The CGM $n_{\rm gas}$ profiles also appear to flatten similarly, which may indicate that the CRs are playing a role in driving outflows via their dynamical coupling to the gas.

In Figure 2, we detailed the fine-grained CR injection rates from AGN and star formation for each `h206` run. These largely show a decreasing $\langle \dot{E}_{\rm cr} \rangle$ with time, where $\langle\rangle$ denotes averaging over some effective transport timescale out to CGM radii. However, there is significant burstiness on short timescales, which depending on the balance of diffusive- versus streaming/advection-like transport will be "smeared out" to varying degrees.

Our current understanding of CR transport physics, which is critical for modulating CGM phase structure, is limited by the lack of direct observables that track CRs and low-density CGM. Moreover, $\epsilon_{\rm cr}^{\rm BH}$ is a highly uncertain quantity, and may also vary in terms of hadronic/leptonic composition (Lin et al. 2023).

FIRE-2 simulations evolved with single-bin treatments of CRs with different physically-motivated sub-grid scattering prescriptions have produced varying CGM properties (Hopkins et al. 2020a; Ponnada et al. 2024a), as have FIRE-3 galaxies evolved with AGN feedback and varied multi-bin CR transport physics (including some explored herein), specifically differing in morphological evolution of the far-infrared-

radio correlation (Ponnada et al. 2025), which may be independently constraining for CR effects in the ISM and inner CGM when compared to spatially resolved observations (Murphy et al. 2006).

Recently, (Hopkins et al. 2025) proposed inverse Compton emission from CR leptons as a method by which to estimate the CR lepton pressure, which is largely tracing the AGN-produced CRs for these simulations at late times (at least within $\sim$1–2 $R_{\rm vir}$ for the $\kappa_{\rm eff}$ modeled here). The distinctions between the $n_{\rm gas}$ and $P_{\rm cr}$ profiles for different $\epsilon_{\rm cr}^{\rm BH}$ (for a fixed CR transport model) appear promising towards constraining $\epsilon_{\rm cr}^{\rm BH}$, but a more statistical sample of simulations and corresponding synthetic observations would be needed to compare against existing constraints, which are often stacked measurements (e.g., from eROSITA Zhang et al. 2024a, 2024b, 2025).

There is also the complementary probe of thermal pressure in the CGM via the thermal Sunyaev–Zel'dovich effect, which when combined with X-ray constraints may be particularly constraining how CRs contribute to galaxy quenching (Ponnada et al. 2026). Quenched massive galaxies appear to be *brighter* in X-rays than their star-forming counterparts with the latest detections (Zhang et al. 2025), while simulations invoking AGN feedback without CRs tend to over-predict the detected halo-integrated tSZ signal by over an order-of-magnitude (Das et al. 2025; Ponnada et al. 2026).

So, by producing synthetic synchrotron (Ponnada et al. 2024b), IR-O/UV (Byrne et al. 2024; Wijers et al. 2024; Qutob et al. 2024; Ponnada et al. 2025), SZ, and X-ray predictions (Chadayammuri et al. 2022; Lu et al. 2026) for feedback parameterized with varied CR injection efficiencies and transport parameterizations, our results suggest we may be able to constrain these physics via observational comparisons of spectrally-resolved CR-MHD simulations with explicit evolution of multi-channel AGN feedback.

While the AGN feedback schemes explored herein have injected the multi-channel feedback energy and momentum on the accretion-kernel scale ($\sim$1–10 pc from the central source), recent developments using idealized setups have suggested that alternative modes of CR injection, e.g., at jet termination shocks (Su et al. 2026), may qualitatively change the quenching and maintenance behavior of a fixed set of feedback parameters in massive galaxies. Our results motivate further exploring such models, building upon those presented herein and in Su et al. (2026) with explicit feedback in a large number of cosmological runs to place detailed constraints on AGN feedback.

Indeed, we have preliminarily explored the SZ and X-ray properties from these simulations. However, while (Hopkins et al. 2025; Ponnada et al. 2026) invoke the CR-feedback driven by AGN to be primarily leptonic, herein we have treated the AGN CR injection spectrum identically to that of SNe injection in terms of initial slope and $p+/e-$ ratio (largely hadronic). Moreover, given the very limited sample, which is by no means extensive in the range of plausible theoretical parameter space, we refrain from drawing any specific conclusions regarding the viability of any specific model. How these observational comparisons constrain models will be the subject of future work.

Finally, we note that structures we see arising in $P_{\rm cr}(r)$ due to time-dependence as well as variation in $\kappa_{\rm eff}$ at large radii may potentially connect to formation of Odd Radio Circles (ORCs) observed in radio surveys around massive galaxies (Norris et al. 2021). Since we have only explored one plausible model for spatially variable CR scattering, we do not perform a comprehensive comparison here, and leave it to future work.

Acknowledgments

Support for C.G., S.P., and P.F.H. was provided by a Simons Investigator Award. S.W. received support from NASA grant 80NSSC24K0838.

Facility: TACC.

Software: astropy (Astropy Collaboration et al. 2013).

Appendix

We calculate $M_{\rm BH}$ and σ as described in Section 2.2 for all snapshots of the VD runs up till $z = 1$ (Figure A1). At late times, all VD runs move along and up the $M_{\rm BH}$–σ relation on average, with small fluctuations in σ. During these times, the galaxy evolution is in "maintenance-mode", where $M_{\rm BH}$ changes slowly and star-formation fluctuates due to the prevention of gas accretion, modifying the central potential and thus σ. We discuss this in more detail in Section 3.2.

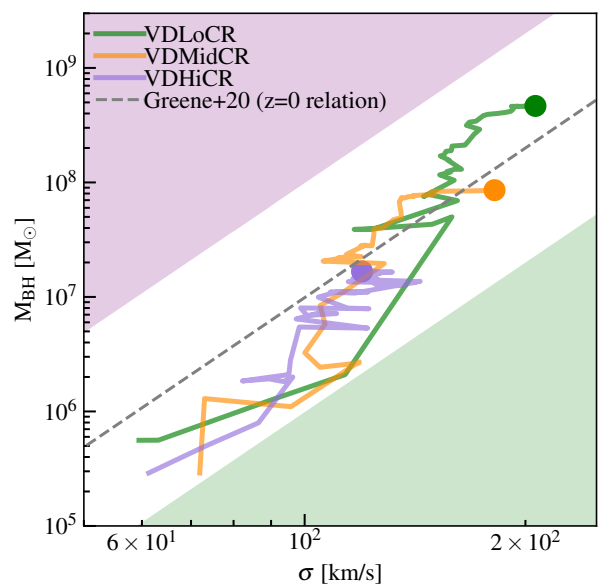

Figure A1. Evolutionary tracks of `h206` VD runs along the $M_{\rm BH}$–σ relation up to their $z = 0$ values, in the style of Figure 1.

ORCID iDs

Charvi Goyal https://orcid.org/0009-0008-8670-3386
Sam B. Ponnada https://orcid.org/0000-0002-7484-2695
Philip F. Hopkins https://orcid.org/0000-0003-3729-1684
Sarah Wellons https://orcid.org/0000-0002-3977-2724
Jose A. Benavides https://orcid.org/0000-0003-1896-0424
Kung-Yi Su https://orcid.org/0000-0003-1598-0083

References

Astropy Collaboration, Robitaille, T. P., Tollerud, E. J., et al. 2013, A&A, 558, A33
Behroozi, P., Wechsler, R. H., Hearin, A. P., & Conroy, C. 2019, MNRAS, 488, 3143
Benson, A. J. 2010, Phys. Rep., 495, 33
Bustard, C., & Zweibel, E. G. 2021, ApJ, 913, 106
Butsky, I. S., Nakum, S., Ponnada, S. B., et al. 2023, MNRAS, 521, 2477
Butsky, I. S., & Quinn, T. R. 2018, ApJ, 868, 108
Byrne, L., Faucher-Giguère, C.-A., Wellons, S., et al. 2024, ApJ, 973, 149
Chadayammuri, U., Bogdan, A., Oppenheimer, B. D., et al. 2022, ApJL, 936, L15
Cole, S., Lacey, C. G., Baugh, C. M., & Frenk, C. S. 2002, MNRAS, 319, 168
Croton, D. J., & Farrar, G. R. 2008, MNRAS, 386, 2285
Croton, D. J., Springel, V., White, S. D. M., et al. 2006, MNRAS, 365, 11
Das, S., Truong, N., Chiang, Y.-K., & Mathur, S. 2025, ApJ, 991, 205
Davé, R., Anglés-Alcázar, D., Narayanan, D., et al. 2019, MNRAS, 486, 2827
Di Matteo, T., Springel, V., & Hernquist, L. 2005, Natur, 433, 604
Fabian, A. C. 2012, ARA&A, 50, 455
Greene, J. E., Strader, J., & Ho, L. C. 2020, ARA&A, 58, 257
Harrison, C. M., & Almeida, C. R. 2024, Galaxies, 12, 17
Harrison, C. M., Costa, T., Tadhunter, C. N., et al. 2018, NatAs, 2, 198
Heckman, T. M., & Best, P. N. 2014, ARA&A, 52, 589
Hopkins, P. F. 2015, MNRAS, 450, 53
Hopkins, P. F. 2025, arXiv:2509.07104
Hopkins, P. F., Butsky, I. S., Panopoulou, G. V., et al. 2022a, MNRAS, 516, 3470
Hopkins, P. F., Chan, T. K., Ji, S., et al. 2021, MNRAS, 501, 3640
Hopkins, P. F., Chan, T. K., Squire, J., et al. 2020a, MNRAS, 501, 3663
Hopkins, P. F., Quataert, E., Ponnada, S. B., & Silich, E. 2025, OJAp, 8, 78
Hopkins, P. F., & Raives, M. J. 2015, MNRAS, 455, 51
Hopkins, P. F., Squire, J., Butsky, I. S., & Ji, S. 2022b, MNRAS, 517, 5413
Hopkins, P. F., Torrey, P., Faucher-Giguère, C.-A., Quataert, E., & Murray, N. 2016, MNRAS, 458, 816
Hopkins, P. F., Strauss, M. A., Hall, P. B., et al. 2004, AJ, 128, 1112
Hopkins, P. F., Wetzel, A., Kereš, D., et al. 2018, MNRAS, 480, 800
Hopkins, P. F., Chan, T. K., Garrison-Kimmel, S., et al. 2020b, MNRAS, 492, 3465
Hopkins, P. F., Wetzel, A., Wheeler, C., et al. 2023, MNRAS, 519, 3154
Jokipii, J. R. 1966, ApJ, 146, 480
Kereš, D., Katz, N., Davé, R., Fardal, M., & Weinberg, D. H. 2009, MNRAS, 396, 2332
Lin, Y.-H., Yang, H.-Y. K., & Owen, E. R. 2023, MNRAS, 520, 963
Longair, M. S. 2008, Galaxy Formation (Springer)
Lu, Y. S., Kereš, D., Hopkins, P. F., et al. 2026, MNRAS, 545, staf1984
Murphy, E. J., Braun, R., Helou, G., et al. 2006, ApJ, 638, 157
Norris, R. P., Crawford, E., & Macgregor, P. 2021, Galax, 9, 83
Ponnada, S. B. 2025, arXiv:2509.02697
Ponnada, S. B., Hopkins, P. F., Lu, Y. S., et al. 2026, ApJ, 997, L13
Ponnada, S. B., Butsky, I. S., Skalidis, R., et al. 2024a, MNRAS, 530, L1
Ponnada, S. B., Panopoulou, G. V., Butsky, I. S., et al. 2024b, MNRAS, 527, 11707
Ponnada, S. B., Cochrane, R. K., Hopkins, P. F., et al. 2025, ApJ, 980, 135
Qutob, N., Emami, R., Su, K.-Y., et al. 2024, ApJ, 977, 72
Ruszkowski, M., & Pfrommer, C. 2023, A&ARv, 31, 4
Ruszkowski, M., Yang, H.-Y. K., & Reynolds, C. S. 2017, ApJ, 844, 13
Salim, S., Rich, R. M., Charlot, S., et al. 2007, ApJS, 173, 267
Schaye, J., Crain, R. A., Bower, R. G., et al. 2014, MNRAS, 446, 521
Sijacki, D., Springel, V., Di Matteo, T., & Hernquist, L. 2007, MNRAS, 380, 877
Sijacki, D., Springel, V., & Haehnelt, M. G. 2009, MNRAS, 400, 100
Sijacki, D., Vogelsberger, M., Genel, S., et al. 2015, MNRAS, 452, 575
Silk, J., & Rees, M. J. 1998, A&A, 331, L1
Somerville, R. S., & Davé, R. 2015, ARA&A, 53, 51
Springel, V., & Hernquist, L. 2003, MNRAS, 339, 312
Su, K.-Y., Bryan, G. L., Hopkins, P. F., et al. 2026, MNRAS, 545, staf2060
Su, K.-Y., Hopkins, P. F., Hayward, C. C., et al. 2019, MNRAS, 487, 4393
Su, K.-Y., Hopkins, P. F., Hayward, C. C., et al. 2020, MNRAS, 491, 1190
Su, K.-Y., Hopkins, P. F., Bryan, G. L., et al. 2021, MNRAS, 507, 175
Su, K.-Y., Bryan, G. L., Hayward, C. C., et al. 2024, MNRAS, 532, 2724
Weinberger, R., Springel, V., Pakmor, R., et al. 2018, MNRAS, 479, 4056
Wellons, S., Faucher-Giguère, C.-A., Hopkins, P. F., et al. 2023, MNRAS, 520, 5394
Wijers, N. A., Faucher-Giguère, C.-A., Stern, J., Byrne, L., & Sultan, I. 2024, ApJ, 973, 99
Zhang, Y., Comparat, J., Ponti, G., et al. 2024a, A&A, 690, A267
Zhang, Y., Comparat, J., Ponti, G., et al. 2024b, A&A, 690, A268
Zhang, Y., Comparat, J., Ponti, G., et al. 2025, A&A, 693, A197